Supplementary Information

Coordinating ionic and electronic conductivity on 3D porous host enabling deep dense lithium deposition toward high-capacity lithium metal anode

Hao Yang[a], Hongfei Zheng[b], Huaming Yu[a], Baihua Qu[c], Libao Chen[a], Jianmin Niu*[d] and Yuejiao Chen*[a]

[a] State Key Laboratory of Powder Metallurgy, Central South University, Changsha, Hunan 410083, PR China

[b] College of Materials, Xiamen University, Xiamen, Fujian 361005, PR China

[c] College of Materials Science and Engineering, Chongqing University, Chongqing, 400044, PR China

[d] Beijing Special Vehicles Research Institute, Beijing 100072, PR China

* Corresponding authors.

E-mail: jmniu168@sohu.com (J. Niu); cyj.strive@csu.edu.cn (Y. Chen)

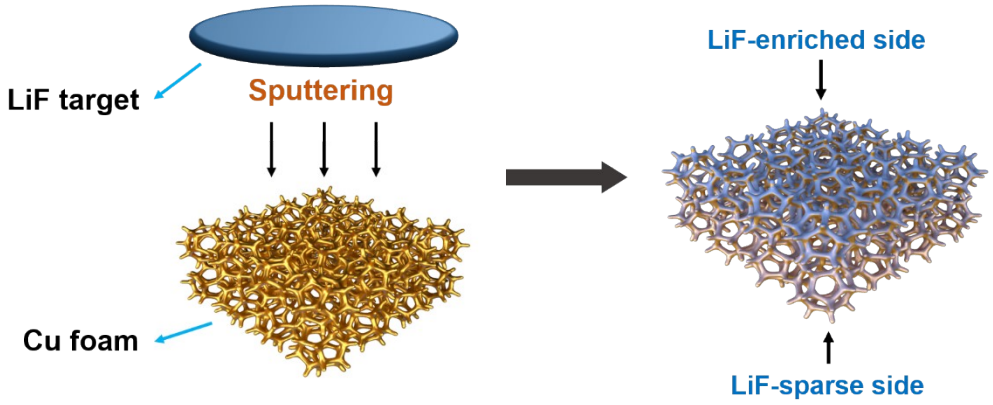

Figure S1. Schematic illustration of the fabrication process. Due to the large pore size and high porosity of copper foam, LiF was sputtered to the interior of Cu foam, thus forming a gradient distribution of LiF from the enriched side to the sparse side.

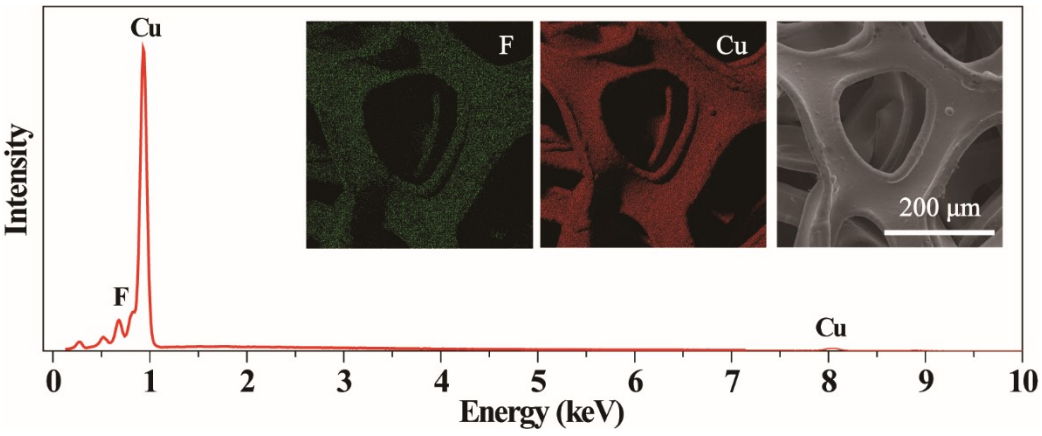

Figure S2. EDS characterization of F and Cu elements on the Cu foam surface with sputtered LiF. The inset images are the distribution mapping of F and Cu elements and the original SEM image from left to right.

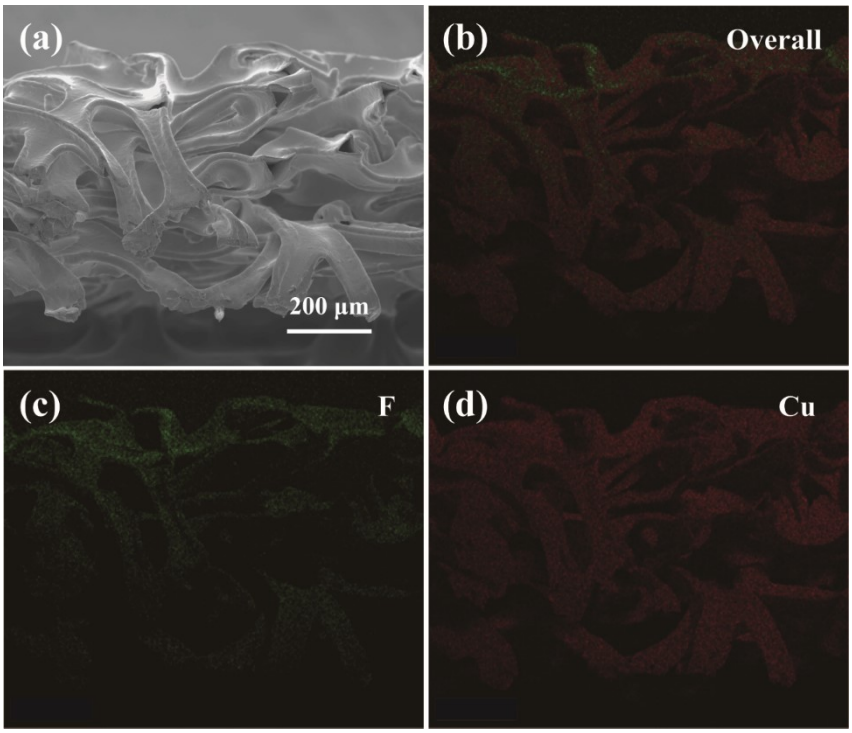

Figure S3. EDS characterization of F and Cu elements on the cross section of the copper foam with sputtered LiF. The signal of the F element from the sputtering direction (from top to bottom) is dense to sparse, indicating the gradient distribution of LiF from top to bottom.

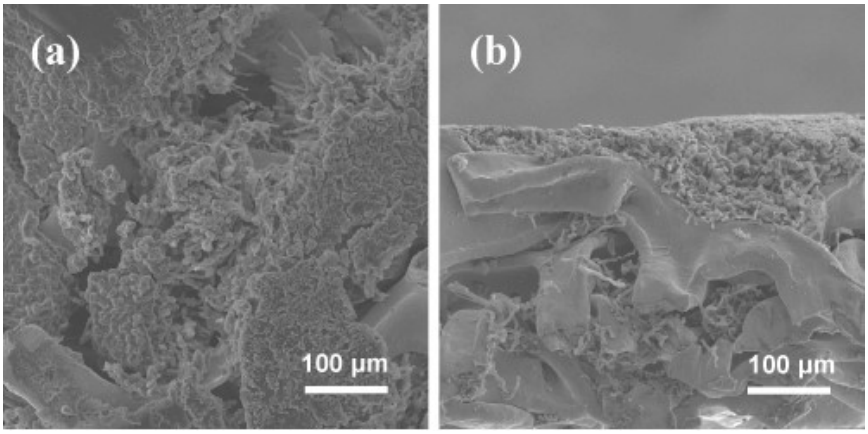

Figure S4. SEM images of pristine Cu foam with lithium deposition of 1 mA h cm^{-2}. (a) Surface view. (b) Cross-sectional view. Obvious Li dendrites and uneven deposition are observed.

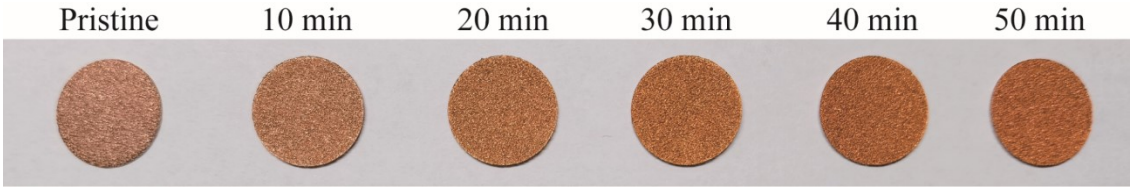

Figure S5. Optical photos before/after LiF sputtering on the surface of Cu foam. With the extension of sputtering time, the color gradually darkens.

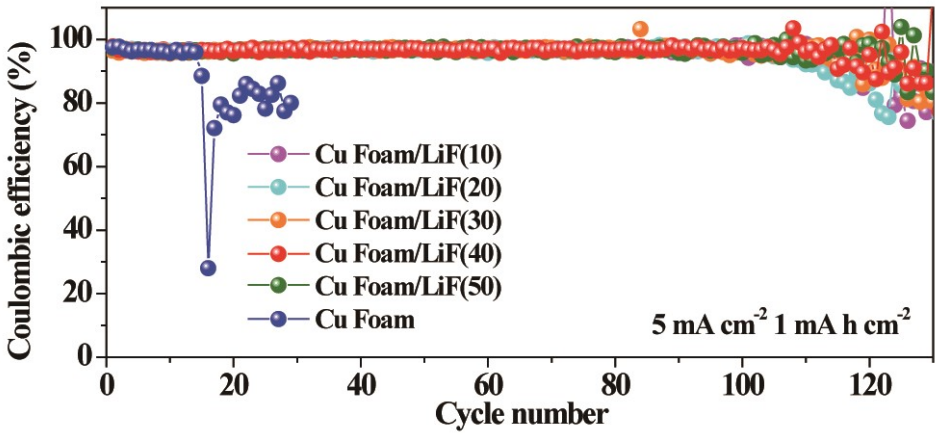

Figure S6. Coulombic efficiency tests for Cu foam with the increasing LiF-sputtering time at the current density of 5 mA cm^{-2} and the capacity of 1 mA h cm^{-2}.

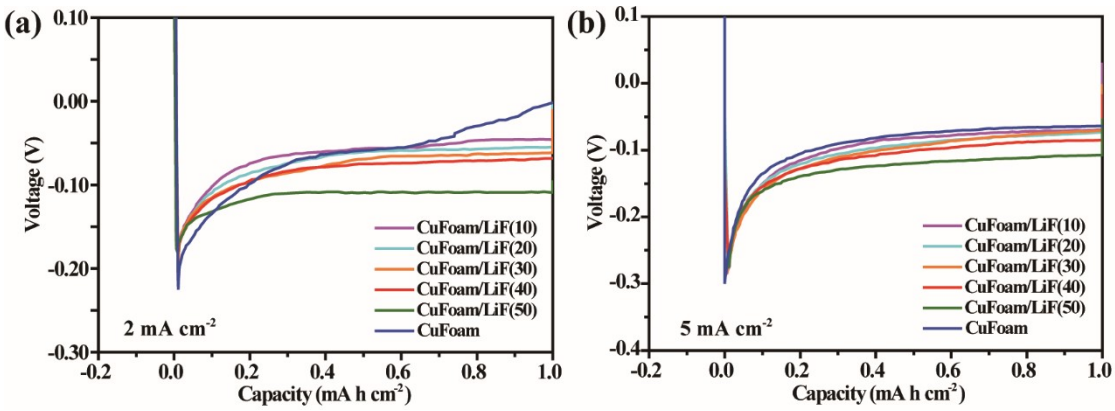

Figure S7. Discharge curves during first cycles in CE tests at different current densities. With the increasing of the sputtering time, the discharge platforms gradually drop.

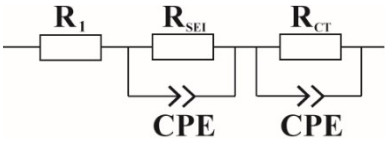

Figure S8. The equivalent circuit for EIS tests.

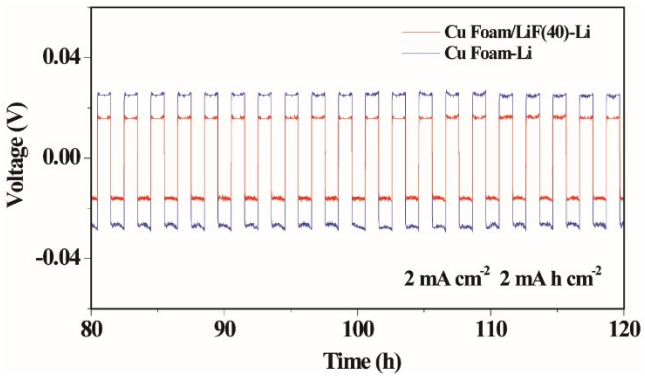

Figure S9. Detailed voltage-time curves of Cu foam/LiF(40)-Li and Cu foam-Li symmetric cells from 80 h to 120 h cycled at 2 mA cm^{-2} for 2 mA h cm^{-2}.

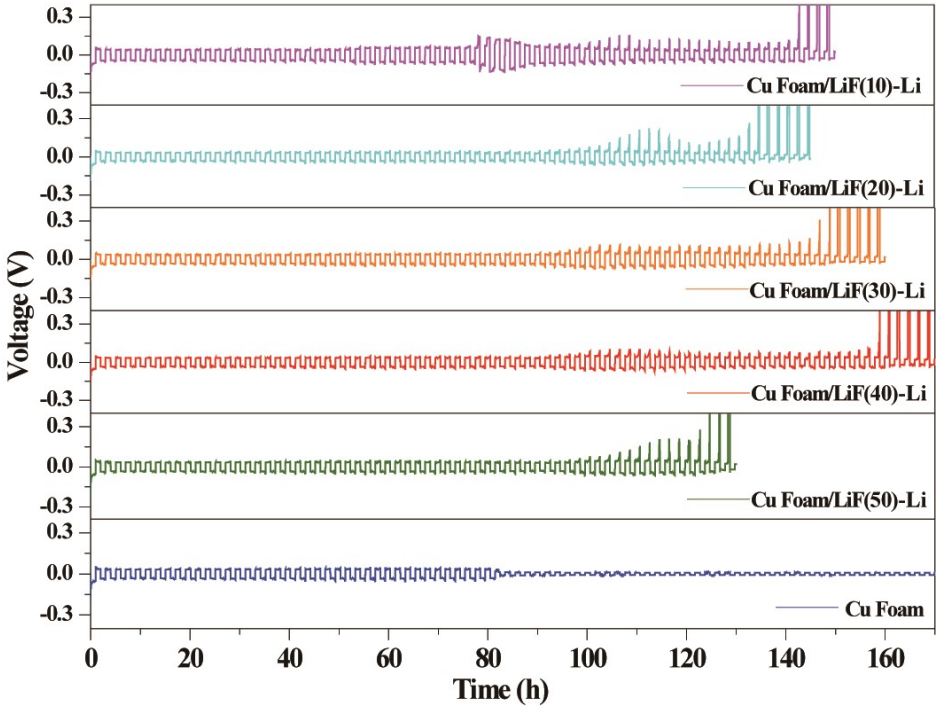

Figure S10. Voltage-time curves of Cu foam-Li symmetric cells with the increasing LiF-sputtering time cycled with the capacity of 5 mA h cm^{-2} at the current density of 5 mA cm^{-2}. The cycle stability of the copper foam-Li symmetric cells with sputtered-LiF are all better than pristine copper foam, and the cell with 40-min LiF sputtering holds the best.

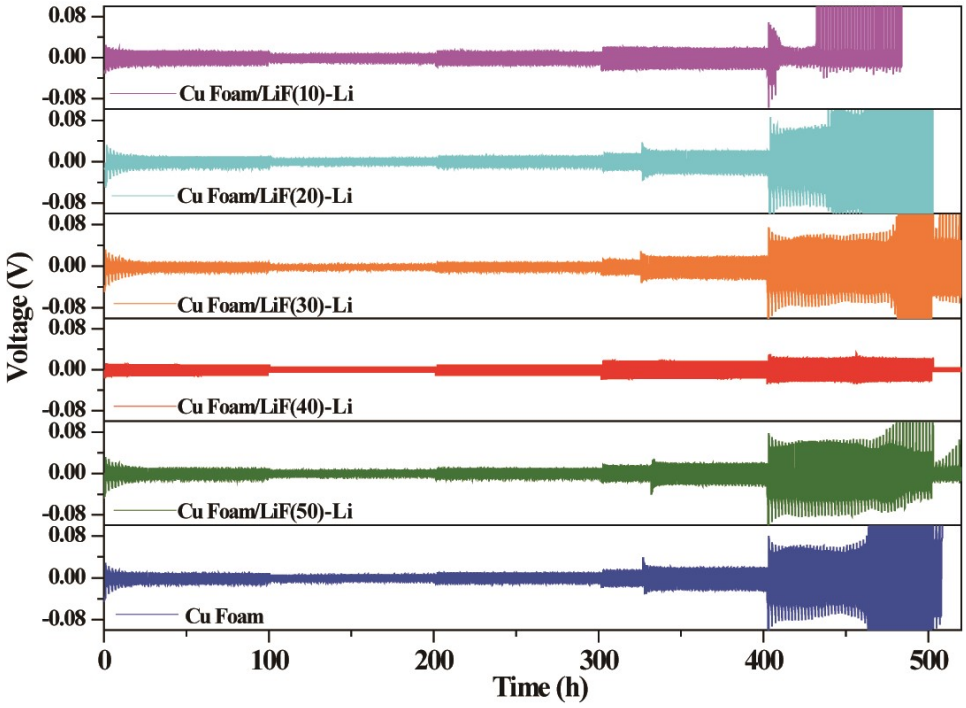

Figure S11. Voltage-time curves of Cu foam-Li symmetric cells with the increasing LiF-sputtering time cycled at different current densities and capacities. The cell with 40-min LiF sputtering holds the best cycle stability.

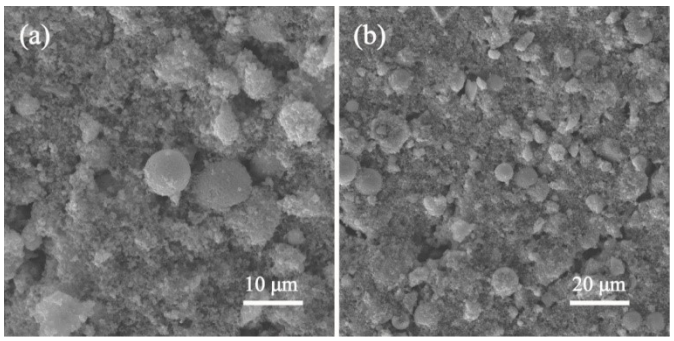

Figure S12. Surface morphologies of the LFP cathode.

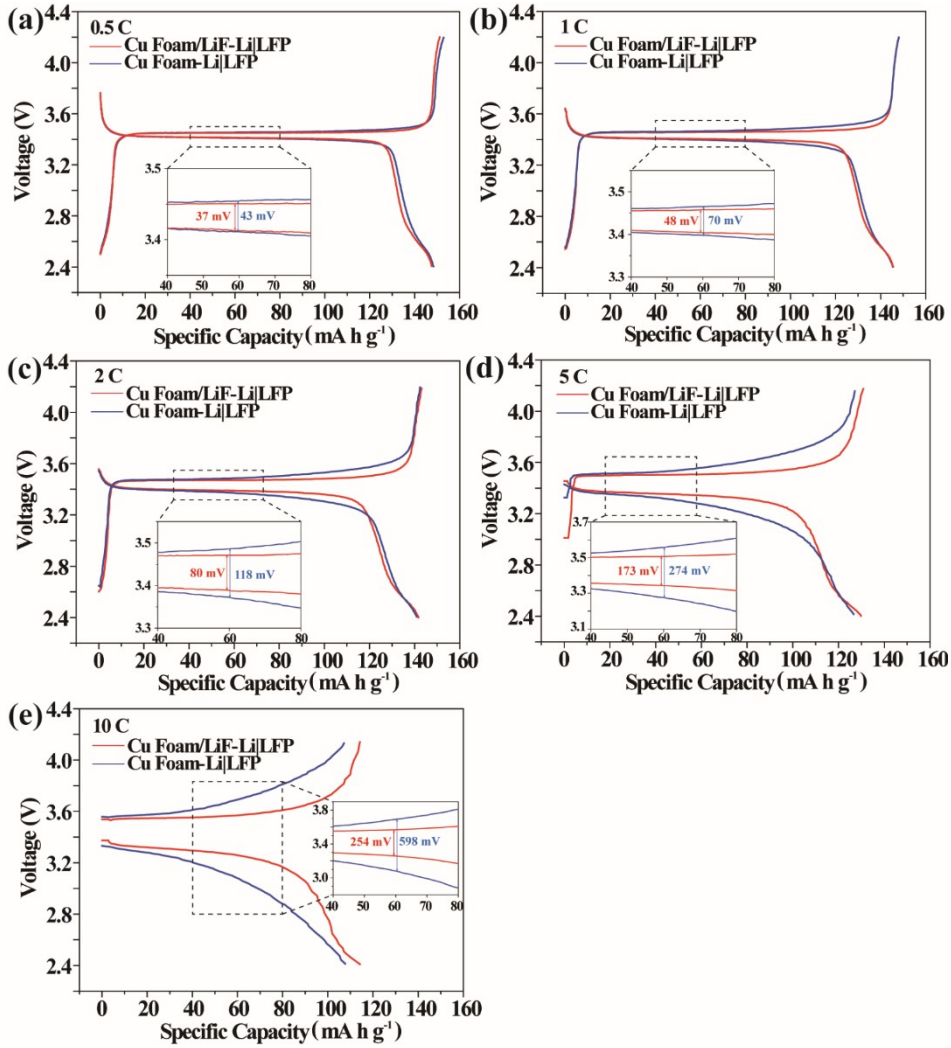

Figure S13. Voltage-capacity curves of Cu foam/LiF-Li|LFP and Cu foam-Li|LFP full cells during charge and discharge processes at different rates.

Table S1. Performance comparison of Cu foam/LiF-Li symmetric cell and other symmetric cells at diverse conditions in previous reports.

Research object	Current density (mA cm^{-2})	Capacity (mA h cm^{-2})	Cycle lifespan for symmetric cell (h)	Ref.
Cu@VG foam	3	3	100	[1]
TiN@Cu foam	3	1	220	[2]
SF-CuNW	3	3	350	[3]
Ag@Cu foam	3	3	400	[4]
CF@ZnO/Na	1	3	500	[5]
LiF@Li matrix	1	1	600	[6]
Li-Cu/Ag	3	0.5	700	[7]
$Ti_3C_2T_x$@Cu	1	1	900	[8]
CCOF	1	1	1000	[9]
Cu foam@NPCN	1	1	1200	[10]
CuFePBA-150	1	1	1800	[11]
Cu foam@GN	0.5	1	2000	[12]
Cu foam/LiF	2	2	1700	This work

References

1. Z. Hu, Z. Li, Z. Xia, T. Jiang, G. Wang, J. Sun, P. Sun, C. Yan and L. Zhang, *Energy Stor. Mater.*, 2019, **22**, 29-39.
2. Y. Wang, W. Zhang, Y. Qi, S. Wang, P. Liu, X. Wei, Y. Yu, W. Sun, X.-Z. Zhao and Y. Liu, *J. Alloys Compd.*, 2021, **874**.
3. A. Fu, C. Wang, J. Peng, M. Su, F. Pei, J. Cui, X. Fang, J. F. Li and N. Zheng, *Adv. Funct. Mater.*, 2021, **31**.
4. L. Wu, W. Jiang, H. Zou, C. Ye, J. Zhang, G. Xu, X. Li, Z. Yue, F. Sun and L. Zhou, *J. Mater. Chem. A*, 2021, **9**, 20748-20757.
5. W. Yang, W. Yang, L. Dong, G. Shao, G. Wang and X. Peng, *Nano Energy*, 2021, **80**.
6. Y. Feng, C. Zhang, B. Li, S. Xiong and J. Song, *J. Mater. Chem. A*, 2019, **7**, 6090-6098.
7. C. Wang, X. Mu, J. Yu, Z. Lu and J. Han, *Chem. Eng. J.*, 2022, **435**.
8. L. Zhang, Q. Jin, K. Zhao, X. Zhang and L. Wu, *ACS Appl. Energy Mater.*, 2022, **5**, 2514-2521.
9. X.-Y. Yue, W.-W. Wang, Q.-C. Wang, J.-K. Meng, X.-X. Wang, Y. Song, Z.-W. Fu, X.-J. Wu and Y.-N. Zhou, *Energy Stor. Mater.*, 2019, **21**, 180-189.
10. F. Pei, A. Fu, W. Ye, J. Peng, X. Fang, M. S. Wang and N. Zheng, *ACS Nano*, 2019, **13**, 8337-8346.
11. Y. Cai, B. Qin, J. Lin, C. Li, X. Si, J. Cao and J. Qi, *ACS Appl. Mater. Interfaces*, 2021, **13**, 23803-23810.
12. G. Yang, J. Chen, P. Xiao, P. O. Agboola, I. Shakir and Y. Xu, *J. Mater. Chem. A*, 2018, **6**, 9899-9905.